32nd Electric Vehicle Symposium (EVS32)
Lyon, France, May 19 - 22, 2019

Comparative Concept Study of Passive Hybrid Energy Storage Systems in 48 V Mild Hybrid Vehicles Varying Lithium-ion Battery and Supercapacitor Technologies

Thorsten Grün, Martin Doppelbauer

Karlsruhe Institute of Technology (KIT), Institute of Electrical Engineering (ETI),
Hermann-von-Helmholtz-Platz 1, 76344 Eggenstein-Leopoldshafen Germany,
thorsten.gruen@kit.edu

Summary

A single energy storage technology will deliver either high power or high energy density. In high cycle applications like 48 V mild hybrid electric vehicles, lithium-ion batteries or supercapacitors have to be oversized to meet power, energy and cycle life requirements. However, a passive hybrid energy storage system is able to meet those challenges but its performance will depend on several factors. In this study, simulations and experimental investigations will show how the design and operation conditions influence the performance of a passive hybridized system. In a comparative study for 48 V systems, consequences on performance are discussed.

Keywords: HEV, lithium battery, supercapacitor, modeling, regenerative braking

1 Introduction

Considering the requirements of an Energy Storage System (ESS) for current generations of 48 V Mild Hybrid Electric Vehicles - MHEV (Gen1: 11 kW; ~320 Wh) [1], a high power to energy (P/E) ratio and a high cycle lifetime is mandatory. Future generations (Gen3: 25 kW; 1 – 3 kWh) of MHEVs will require a different P/E ratio in order to enable pure electric driving within cities (FHEV = Full Hybrid Electric Vehicle) [2]. Lithium-ion Batteries (LIB) in form of high-energy (HE) or high-power (HP) cells and even supercapacitors (SC) as a single system cannot satisfy all requirements in terms of P/E ratio and cycle life without oversizing and/or overstraining the system. Therefore, a Hybrid Energy Storage System (HESS), and specifically a passive HESS is a suitable approach for pulse load profiles, which appear in MHEVs and even FHEVs.

Passive HESS show higher efficiencies and reduced complexity than other HESS solutions [3]. However, their performance is mainly determined by the technology matching in terms of voltage characteristics and ohmic resistance ratio whereas new degrees of freedom arise on system level. Different LIB technologies and even more so conventional Electrochemical Double Layer Capacitors (EDLC) exhibit quite different characteristics in ohmic resistances and voltages. New capacitor technologies like Lithium-carbon Capacitors (LIC) [4]–[6] arise that fill the gap in power and energy density between LIB and SC technologies and bring new flexibilities in the design of passive HESS.

This study shows by experimental and model-based investigations how the design of a passive HESS and its operation condition influence power and energy density. Advantages over battery-only ESSs are discussed in a comparative study by analyzing two virtual 48 V MHEV scenarios.

2 Fundamentals

2.1 Pulse current load and operating voltage

Factors that have an impact on the performance of a HESS within pulse load profiles have already been discussed in previous papers. Besides the setup and the capacity ratio of the LIB or the SC [6], [7], also the characteristic of the pulse load profile and its impact were part of the discussion [8], [9].

The character of a pulse load profile can be described by its period T and the pulse duration PD, in which the load current I_{load} is active. In Fig. 1 (a) a given current versus time $I_{load}(t)$ is presented schematically for two different periods (T_1 and T_2) as well as for two different pulse durations (PD_1 and PD_2). Using Eq. 1 the pulse profile can be characterized by its duty cycle DC, which describes the relationship between the period T and the pulse duration PD.

$$DC = \frac{PD}{T} \tag{1}$$

The individual voltage limits of two hybridized energy storage technologies determine the permissible voltage operating range. The upper cut-off voltage (U_{max}) and the lower cut-off voltage (U_{min}), which is violated first, determine the actual operating range of the HESS and in consequence the usable energy of each energy storage technology (see Fig. 1 (b)).

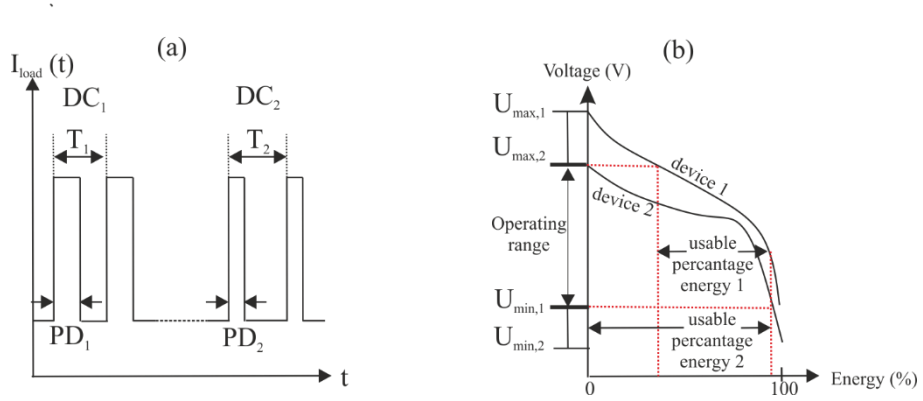

Figure 1: (a) Schematic of pulse load profile with two different characteristics in pulse duration PD and period T resulting in two different duty cycles DC; (b) Representation of upper and lower cut-off voltages (U_{max} and U_{min}) on the operational voltage range of a passive HESS and usable energy of each component

2.2 Characterization of ESS during pulse load profiles

Energy and power density are typical dimensions to describe the characteristics of an ESS. The energy density e_{ESS} defines which energy can be extracted per mass m_{ESS} of the ESS. In [10] it is proposed to integrate time-varying voltage U(t) and current load $I_{load}(t)$ only during active pulses (g=1) and to neglect U(t) and $I_{load}(t)$ during pulse off times (g=0). To characterize the power density p_{ESS}, e_{ESS} is divided by the product of total time τ and D, whereby D is the fraction of τ in which the current pulse is active. The energy density e_{ESS} and the power density p_{ESS} can be calculated by Eq. 2 – 3:

$$e_{ESS} = \frac{1}{m_{ESS}} \int_0^{\tau} U(t) \cdot I_{load}(t) \cdot g(t) \tag{2}$$

$$p_{ESS} = \frac{e_{ESS}}{\tau D} \tag{3}$$

The P/E ratio is a unit-less dimension, which describes the ratio between power and energy density of an ESS and it's also used to specify the requirements of P/E ratio for applications. Exemplary for HEV the P/E ratio is 15 [11], which means that the necessary power requirements are 15 times higher than the required energy.

3 Modeling

It is one objective of this study to derive a universal cell model (CM) for a variety of LIB and SC technologies along with a standardized parameter determination, which simplifies the design processes for HESSs. Besides commercial LIBs, such as lithium-ion phosphate (LFP) and lithium-ion cobalt oxide (LCO), conventional EDLC technologies and two different types of LIC technologies are also investigated in this study.

There are two general concepts that use both LIB and SC materials for the electrodes, either as a serial or parallel connection. The composition of the electrodes differs between the two concepts. In serial connection, one electrode consists of battery material and the other one holds EDLC material and form a serial hybrid capacitor (SHC). A parallel hybrid capacitor (PHC) consists of so-called bi-material electrodes which are containing EDLC and battery material [12].

3.1 Cell model (CM)

The Thevenin model is used as the cell model. This is a common method to describe the electrical behavior of LIBs [13], [14]. Considering state of the art modeling of EDLCs, the Thevenin model is similar to the "classical model" for EDLCs [15], but extended by a voltage source.

The model consists of a voltage source to represent the open circuit voltage (OCV) U_{ocv}, the ohmic resistance R_{inter} which describes the ohmic losses due to electrolyte and electrodes and one RC-circuit (with R_{RC} and C_{RC}) to take diffusion processes within electrochemical energy storage devices into account. The electrical circuit model (ECM) is presented in Fig. 3 (a). The terminal voltage U_{cell} can be calculated by Eq. 4 considering the dynamics of U_{RC} between two time samples Δt in Eq. 5.

$$U_{cell}(t) = U_{OCV}(t) + I(t) \cdot R_{inter}(t) + U_{RC}(t) \tag{4}$$

$$U_{RC}(t) = U_{RC}(t-1)e^{\frac{-\Delta t}{R_{RC}(t)C_{RC}(t)}} + (1 - e^{\frac{-\Delta t}{R_{RC}(t)C_{RC}(t)}})R_{RC} \cdot I(t-1) \tag{5}$$

3.2 Single cell characteristics and parameter determination

R_{inter} is determined by the R_{DC} pulse method [16] in which the pulse duration PD is varied depending on the cell technology. Using Ohm's law, R_{inter} can be calculated from the resulting change in voltage caused by the applied current. This procedure is performed for a State of Charge (SOC) of 10 – 90 % in 10 % steps in discharge (DIS) direction and will be used as a look-up table within the simulation tool. For LIBs, the pulse is performed for 20 sec and for all SC technologies, R_{inter} given in the datasheets are reached by a 2 sec pulse.

The parameterization procedure of U_{OCV} is slightly different between cell technologies. For LIB and LIC_{PHC}, U_{OCV} is measured in a 2.5 % SOC interval starting from 100 % SOC and a relaxation time of 20 mins after each point interval is reached. In case of EDLC and LIC_{SHC}, U_{OCV} is measured by a continuous 1 C charge starting at U_{min} until U_{max}. Measured parameters for modeling U_{OCV} and R_{inter} characteristics are given in Fig. 2. R_{RC} and C_{RC} are determined by using Matlab® Optimization Toolbox in which a nonlinear Levenberg-Marquardt algorithm is used to fit the parameters R_{RC} and C_{RC} in the least square sense to minimize modeled and measured error of U_{cell}.

Besides the high-energy versions of LIBs (LFP_{HE} and LCO), also a high-power oriented LFP cell (LFP_{HP}) is parameterized for the virtual concept study. To analyze energy and power density, each cell is charged by a 1 C constant-current-constant-voltage (CCCV) regime until the upper cut-off voltage U_{max} and a cut-off current of C/20 are reached. Afterwards, each cell is discharged with a pulse load profile with a duty cycle DC of 0.5 at pulse duration PD set to 10 sec until the lower cut-off voltage U_{min} is reached. In general, power densities consider mainly maximum allowed C-Rates in DIS direction, which for most LIBs are higher than in charge (CHG) direction. One of the most crucial design constraints in ESS design of MHEVs are the high

peak currents in CHG direction (~230 A for 11 kW at 48 V). Hence, for power and energy density measurement, the highest allowed C-Rates for CHG direction are applied.

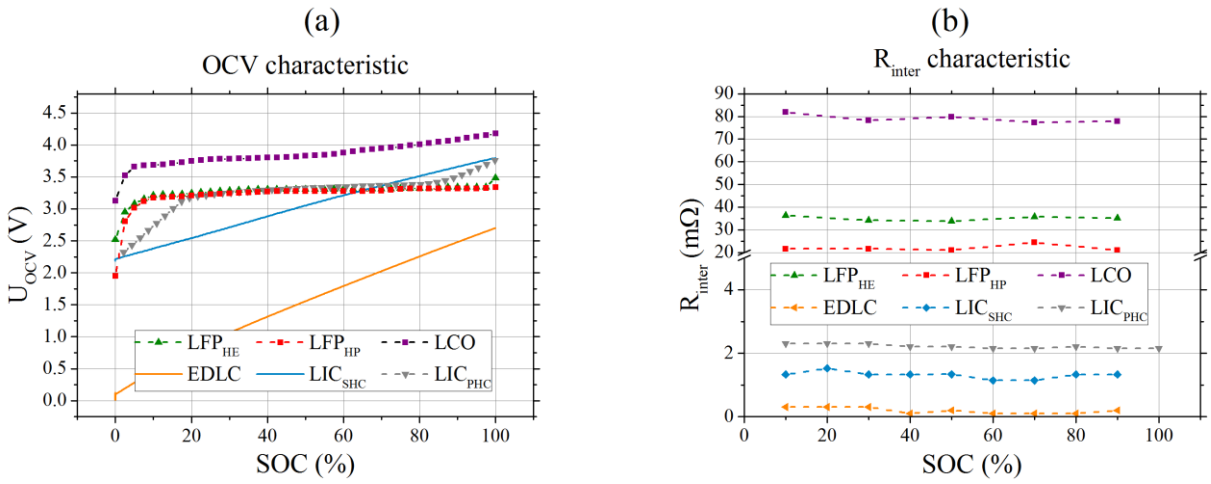

Figure 2: Measured parameter for cells under study; (a) Measured OCV characteristics for LIB and SC; (b) R_{inter} characteristics for OCV and SC technology with R_{DC} pulse measurement

The technical data of all cells under study are given in Table 1 including maximum C-Rate for CHG direction according to the data sheets. Measured power and energy density for abovementioned test procedure and using Eq. 2-3 are added with indices implicating the cell type (HE, HP, SHC, PHC).

Table 1: Technical data of cells under study including measured energy/power densities and capacities

Cell type	Cell design	Capacity (Ah)	Voltage range (V)	Mass (kg)	Volume (l)	C-Rate max CHG	e_{ESS} Whkg^{-1}	p_{ESS} Wkg^{-1}
LCO	18650	2.45	2.5 – 4.2	0.045	0.017	0.75	209.45	149.71
LFP_{HE}	26650	3.00	2.0 – 3.6	0.085	0.036	1	109.54	109.89
LIC_{SHC}	Pouch	1.28	2.2 – 3.8	0.280	0.150	117	11.12	1585.12
LIC_{PHC}	Pouch	4.30	2.2 – 3.8	0.270	0.150	35	35.13	1123.57
EDLC	Cylindrical	2.25	0.1 – 2.7	0.540	0.390	471	2.27	738.46*
LFP_{HP}	26650	2.50	2.0 – 3.6	0.076	0.036	4	101.14	411.98

* Maximum allowed C-Rate couldn't be supplied due to test bench limitation (max 200 A). A higher p_{ESS} is possible

3.3 From cell model (CM) to system model (SM)

In a battery pack many cells are connected in a hierarchal manner by serial and/or parallel connection (xSyP) to meet the voltage, power and/or energy requirements of the application. To derive a system model (SM) from a cell model, the parameters of the cell model are scaled up according to the configuration (xSyP) to emulate the time dependent voltage and resistance characteristics of the system (see Eq. 6). The indices (LIB, SC) imply the considered technology. This method is quite accurate as long as no intrinsic cell imbalances are assumed [17]. Calmer's rule is applied to solve Eq. 6 for I_{LIB} and according to Kirchhoff's current law, the current of the SC bank I_{SC} can be calculated from the difference between I_{LIB} and I_{load} given in Eq. 7.

$$\begin{bmatrix} 1 & 0 \\ \left(-R_{inter,SC}(t)\cdot\frac{S_{SC}}{P_{SC}}\right) & \left[\left(R_{\mathrm{inter,SC}}(t)\cdot\frac{S_{SC}}{P_{SC}}\right)+\left(R_{\mathrm{inter,LIB}}(t)\cdot\frac{S_{LIB}}{P_{LIB}}\right)\right] \end{bmatrix} \begin{pmatrix} I_{\mathrm{load}}(t) \\ I_{\mathrm{LIB}}(t) \end{pmatrix} = \begin{pmatrix} I_{\mathrm{load}}(t) \\ \left(U_{\mathrm{OCV,LIB}}(t)+U_{\mathrm{RC,LIB}}(t)\right)S_{\mathrm{LIB}}-\left(U_{\mathrm{OCV,SC}}(t)+U_{\mathrm{RC,SC}}(t)\right)S_{\mathrm{SC}} \end{pmatrix} \quad (6)$$

$$I_{\mathrm{SC}}(t) = I_{load}(t) - I_{\mathrm{LIB}}(t) \quad (7)$$

As the currents in Eq. 6-7 are calculated on the system level, the changing SOC must be considered within the cell model. To accomplish this, the current I of each bank is divided by the product of each nominal capacity in ampere-hours (Ah) C_N of a cell and by the number of cells P that are connected in parallel. The time-varying SOC(t) is updated iteratively between two time steps Δt according to Eq. 8:

$$SOC(t) = SOC(t-1) + \frac{I(t-1) \cdot \Delta t}{C_N \cdot P} \cdot 100\% \tag{8}$$

An overview of the algorithm containing upscaling the cell model parameters along with the calculation of load distribution and a drawback to parameter dynamics is given in Fig. 3 (b).

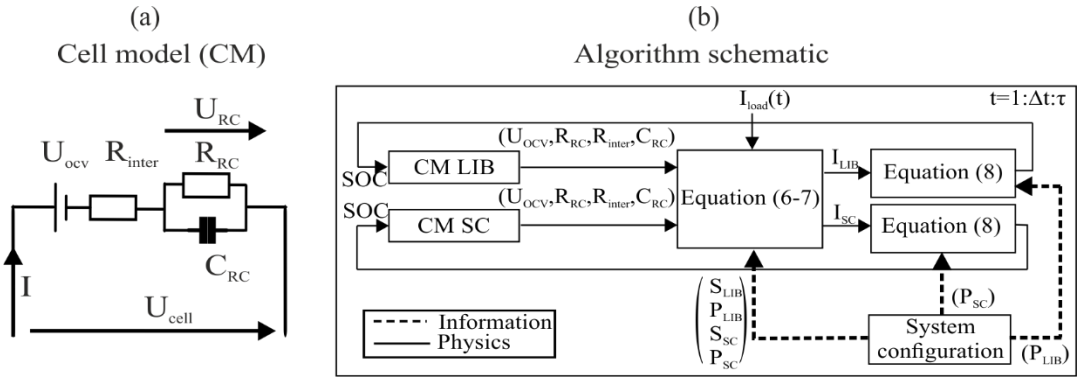

Figure 3: Schematics of the cell model (a) and the algorithm for system modeling (b)

4 Analysis

The analysis of passive HESS is conducted by experimental and model-based approaches. Within experimental investigations, LIB and SC technologies are hybridized on cell level (C2C) and on a 48 V system level (S2S). In focus are the energy and power density depending on technology matching, the system layout and the impact of pulse load characteristics. To derive further findings of practical applicability of HESS, model-based analysis of nowadays (Gen1) and future-oriented (Gen3) MHEV applications are conducted.

4.1 Experimental study of energy density and power density enhancement

The determination of energy and power density of HESSs on C2C and S2S level is conducted in the same way as for the single cells (PD: 10 sec; DC: 0.5). Besides that, for S2S study, pulse duration PD and duty cycle DC are changed according to the pulse duration and the duty cycle occurrence in application-oriented load profiles. For evaluating power density, only results, in which I_{LIB} isn't exceeding its maximum allowed C-Rate counterpart, are taken into account. For the calculation of energy and power density Eq. 2-3 are applied, whereas for S2S analysis only the cumulated mass of the used cells is considered to calculate m_{ESS}.

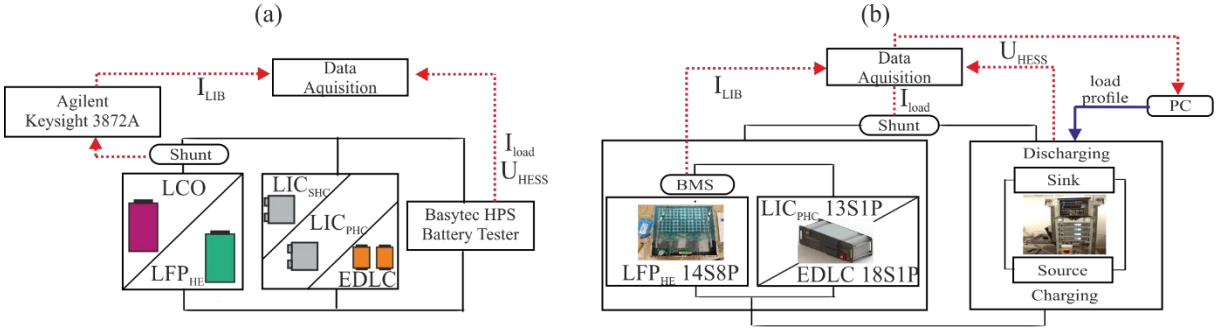

Figure 4: (a) Setup and schematic of C2C campaign with data acquisition; (b) Setup and schematic of S2S campaign using ESS of Table 2

4.1.1 Cell to Cell analysis (C2C)

A Basytec HPS Battery Tester is used for the C2C experiments to provide I_{load} (PD: 10 sec; DC: 0.5) and to measure the terminal voltage of the HESS U_{HESS}. An Agilent Keysight 3872A measures the voltage drop over a shunt resistance (1 mΩ) to identify I_{LIB} and I_{SC}. With Ohm´s law, I_{LIB} can be determined directly. Using Eq. 7, I_{SC} can be calculated by using measurement data of I_{LIB} and I_{load} with a time resolution of 1 sec. As HESS, LFP_{HE} and LCO are connected to all SC technologies under study. In the case of the EDLC, two EDLC have to be connected in serial to gain the voltage ranges of LIBs. The schematics of the test bench and data acquisition are presented in Fig. 4 (a).

4.1.2 System to System analysis (S2S)

For investigations on a S2S level, sinks and loads are used (cumulated max. 120 A CHG/DIS), whose load profiles can be controlled by a PC. As for the C2C investigation, a shunt resistance (1 mΩ) is used to determine I_{load} in a time resolution of 0.2 sec. In comparison to the C2C level, a Battery Management System (BMS) is necessary to satisfy safety requirements of the used 48 V ESS, which is also providing data like I_{LIB} for the evaluation and calculating I_{SC} according to Eq. 7.

In application-oriented profiles, like HEV life cycle test in Fig. 5 (a), a variety of pulse durations and duty cycles can be found. Therefore conspicuous peak powers, like 11 kW peak power, are investigated in terms of its pulse duration and duty cycle. For 11 kW peaks, an average pulse duration of 2 sec at an average duty cycle of 0.03 occurs. Besides 2 and 10 sec pulse durations, also 5 sec is as pulse duration considered, hence following instructions of [1], ESS for MHEV applications should enable maximum power for 5 sec.

The 48 V systems of LFP_{HE} and LIC_{PHC} are built as prototypes. For the 48 V EDLC system, a commercially available product is used. Energy and power densities are identified by the abovementioned regime and are presented in Table 2 along with measured capacities for a 1 A DIS after a 1 C CCCV CHG regime. Data acquisition, control and analysis are accomplished using LabVIEW ®. Four HEA-PSI91000-030U3 are used as sink and four HEA-ELR91500-030 from company Heidenpower are used as load. Data acquisition hardware components include one Q.gat_IP controller, Q.bloxx_A107 with four universal analog input channels and Q.bloxx_A127 with four voltage input channels from Gantner Instruments.

Table 2: Technical data of 48 V ESS under study

System / Parameter	Topology	Voltage range (V)	Capacity (Ah)	e_{ESS} $Whkg^{-1}$	p_{ESS} Wkg^{-1}
LFP_{HE}	14S8P	32.0 – 48.5	22.45	103.08	99.67
LIC_{PHC}	13S1P	30.7 – 47.5	3.46	21.69	1328.20*
EDLC	18S1P	0.1 – 48	2.22	1.47	538.55*

* Maximum current couldn't be supplied due to test bench limitation (max 120 A). A higher p_{ESS} is possible

4.2 Model validation and virtual concept study

4.2.1 Model validation

The model is validated by using the normalized-root-mean-square error (NRMSE) method. Firstly, simulated and measured voltages U_{cell} of the cell model during dynamic load profiles are validated. Secondly, the model accuracy in terms of I_{LIB}, I_{SC} and terminal voltage U_{HESS} of each HESS within C2C campaign for a constant load followed by a pulse load profile is investigated. At last I_{LIB}, I_{SC} and the terminal voltage on S2S level U_{HESS} are also validated by experiments of the S2S campaign (see Fig. 7). Calculated errors of I_{LIB} and I_{SC} are normalized to the range of maximum measured current in CHG and DIS of each. Voltage errors are normalized to the arithmetic mean value of measured terminal voltages U_{HESS} or U_{cell} respectively. Finally, NRMSE of SC and LIB are summarized as overall model accuracy by calculating arithmetic mean errors of current and voltage for each validation campaign.

4.2.2 Virtual concept study for two MHEV scenarios (Gen1 – Gen3)

In the virtual concept study, the performance of HESS and commercial ESS using high-power or high-energy should be compared within realistic scenarios. The first study shall represent nowadays requirements for MHEV ESS. These are start-stop, regenerative braking, and acceleration tasks. For this simulation, the load profile of Fig. 5 (a) from the United States Advanced Battery Consortium (USABC) is used. The second study represents future tasks of MHEV, which involve additionally pure electric inner city driving. Thus, the given acceleration a and velocity v profiles of the WLTP are converted into a power profile P_v by Eq. 9 and using parameters of Table 3.

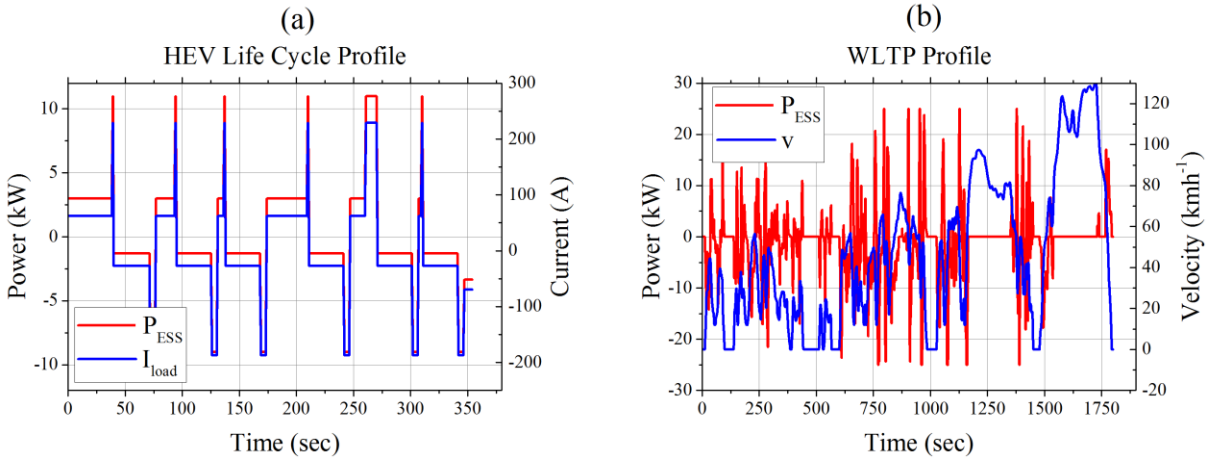

Figure 5: Profiles of virtual concept study; (a) Power and current for HEV Life Cycle Profile proposed by USABC for nowadays MHEV; (b) Velocity profile of WLTP and computed ESS power to emulate future MHEV with inner-city driving mode

Table 3: Parameters for load profile computation for Gen3 emulation

Mass of vehicle m_v (kg)	Gravitational acceleration g (m s^{-1})	Rolling resistance C_r (-)	Density of air ρ_{air} (kg m^{-3})	Drag coefficient C_d (-)	Cross-sectional area A_{front} (m^2)	ESS max CHG/DIS Power (kW)
1615	9.81	0.01	1.22	0.30	2.30	25

The Energy Management System (EMS) controls how a MHEV splits the power supply to the combustion engine (CE) and/or the ESS (see Eq. 10). Thus, a first-order approach is assumed following the regime described in Table 4 to emulate P_{ESS}. The input parameter $I_{Load}(t)$ of the model is computed by $P_{ESS}(t)/48$ V.

$$P_v = \left(m_v \cdot a + m_v \cdot g \cdot C_r + \frac{1}{2}\rho_{air} \cdot C_d \cdot A_{front} \cdot v^2\right) v \tag{9}$$

$$P_v = P_{CE} + P_{ESS} \tag{10}$$

Table 4: Energy Management System (EMS) for MHEV application of Gen 3

Mode	Condition	Description
Inner City Driving	v< 50 kmh^{-1}	P_v is powered by ESS
Engine Mode	50 kmh^{-1}< v < 70 kmh^{-1}	P_v is powered by ESS and CE Linear decrease of P_{ESS} at 50 kmh^{-1} to 0 kW at 70 kmh^{-1} is assumed
Freeway Mode	v>70 kmh^{-1}	P_v powered by CE
Regenerative Braking	a<0	Until 25 kW ESS is getting charged

The model-based investigation is divided into four studies, which are comparing weight and volume of a HESS and its competitive ESS as well as the energy throughput Q_{TP} of a single cell within a HESS and its competitive ESS. The number of serial cells is determined by the system voltage of 48 V whereas the number of parallel cells is dictated by the maximum C-Rate for each technology (see Table 1) and the maximum peak

of I_{load}. In general, those LIBs aren't typical representatives of commonly used LIBs in automotive applications. However, the principle objective of this study is to determine if there are possible configurations of HESS with HE cells that can compete with HP ESS. Another objective is to determine how existing ESS can be improved by a passive hybridization. A number of virtual HESS and ESS with LFP are set up according to Table 5. Only LFP-LIB comparable high-energy and high-power versions in cell type and format are part of the study.

Table 5: Technical data of virtual (H)ESS within the concept study

Study	Study 1	Study 2	Study 3	Study 4
Profile	HEV	HEV	WLTP	WLTP
HESS setup				
LIB bank (xSyP)	LFP_{HE}14S2P	LFP_{HP}14S10P	LFP_{HE}14S90P	LFP_{HP}14S40P
SC bank (xSyP)	LIC_{PHC}13S6P	LIC_{PHC}13S2P	LIC_{PHC}13S10P	LIC_{PHC}13S1P
HESS weight (kg)	23.44	17.52	142.20	45.51
HESS volume (l)	12.85	8.98	65.09	22.13
HESS capacity (kWh)	1.1	1.5	14.4	4.5
ESS setup	LFP_{HP}14S23P	LFP_{HP}14S23P	LFP_{HE}14S174P	LFP_{HP}14S53P
ESS weight (kg)	25.54	25.54	207.06	56.39
ESS volume (l)	12.10	12.10	87.70	26.71
ESS capacity (kWh)	2.9	2.9	26.3	6.7

5 Results

5.1 Experimental results

Energy density and power density of HESS spread for a pulse duration PD of 10 sec with duty cycle DC of 0.5 from 9.5 up to 55.4 Whkg^{-1} and 9.7 to 65.8 Wkg^{-1} on C2C level (see Fig. 6 (a)). Highest energy and power density values are achieved by HESS existing of LFP_{HE} and LIC_{PHC} (55.4 Whkg^{-1}; 65.8 Wkg^{-1}). Considering LCO HESS, using LIC_{PHC} are leading to the highest e_{ESS} for LCO HESS as well.

In the comparison of LFP_{HE}-EDLC HESS on C2C to S2S level, it can be seen, that power and energy density are increasing by more than a factor of 5. In the case of LFP_{HE}-LIC_{PHC} HESS, the factor of increasing power and energy density is approx. 1.5 and with 84.5 Whkg^{-1} and 110 Wkg^{-1} highest values of energy and power density of all HESS are achieved for 10 sec pulse duration at a duty cycle of 0.5.

Changing the pulse duration PD from 10 to 2 sec at a duty cycle DC of 0.03, power density is increasing for both HESS in S2S campaign by maintaining constant energy density at the same time (see Fig. 6 (b)). Power densities at 2 sec pulse duration are for LFP_{HE}-EDLC HESS 169 Wkg^{-1} and for LFP_{HE}-LIC_{PHC} HESS 194 Wkg^{-1}, whereas for LFP_{HE}-LIC_{PHC} HESS the difference in power density between 5 sec and 2 sec pulse duration is only approx. 10 Wkg^{-1}. Compared to 48 V LFP ESS, its an increase in power density up to a factor of 1.9 by a reduction of energy density up to 14 %.

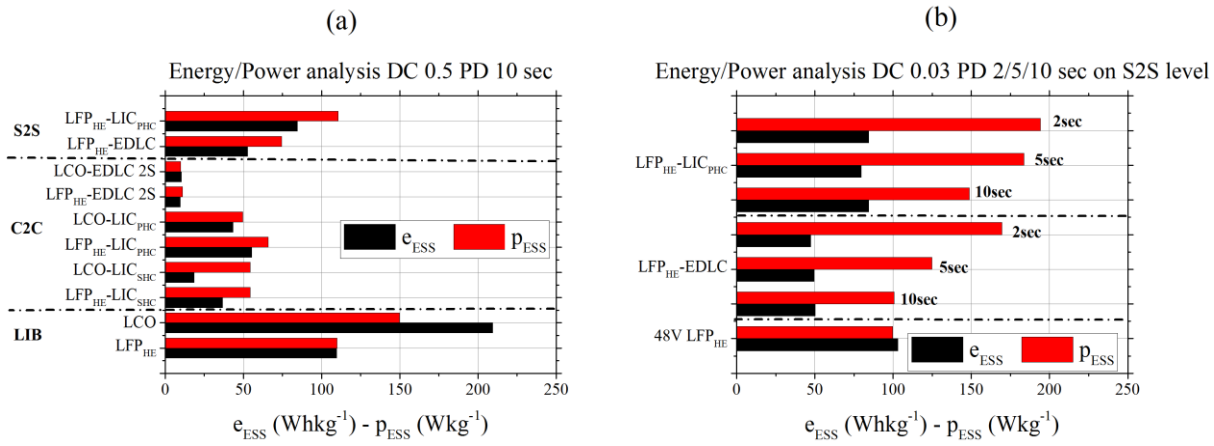

Figure 6: (a) Energy and power density analysis for C2C and S2S campaign at PD 10 sec and DC of 0.5; (a) Energy and power density analysis for S2S campaign at constant DC of 0.03 and load pulses of 2, 5 and 10 sec PD

5.2 Model validation

Exemplary profiles of the validation campaign for the cell and the system model on a C2C and S2S level are given in Fig. 7. The average overall accuracy of the model for each campaign and the number of considered errors is presented in Table 6. Voltage error increases from 1.95 % for the cell model CM up to 3.44 % for S2S analysis. The model error of the electrical current shows a similar trend. Herein, the mean error increases from C2C analysis to S2S analysis from 6.33 to 7.42 %.

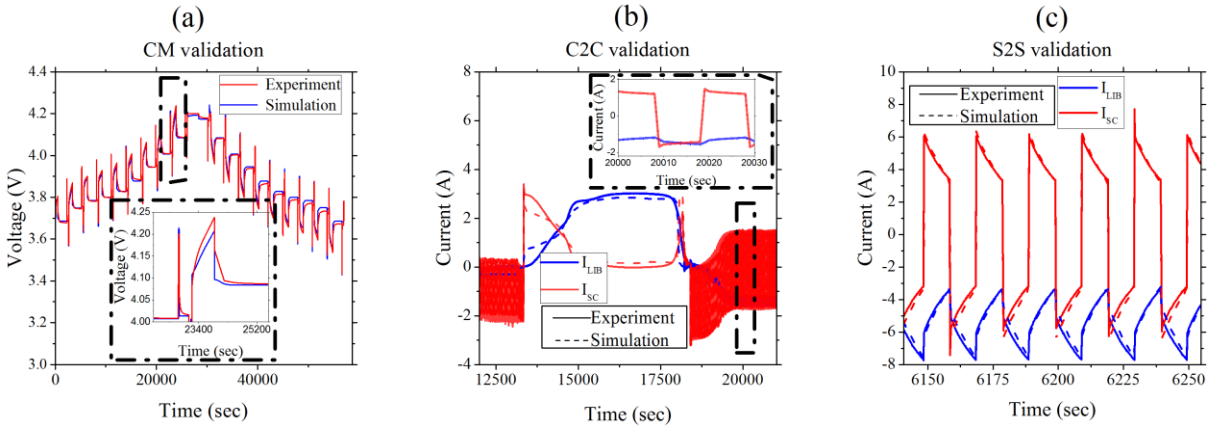

Figure 7: Measured and simulated currents and terminal voltage profiles; (a) Measured and simulated voltage behavior of LCO; (b) Modeled and measured current profile of LFP_{HE}-LIC_{SHC} HESS of C2C campaign; (c) Modeled and measured current profile of LFP_{HE}-EDLC hybrid of S2S campaign

Table 6: Average overall model accuracy for CM, C2C and S2S analysis given as NRMSE

Campaign	Number of errors	Voltage (%)	Current (%)
CM	6	1.95	-
C2C	12	2.94	6.33
S2S	4	3.44	7.42

5.3 Results of virtual concept study

The results of the comparative virtual concept study given in Fig. 8 show that the weight and volume of a HESS can be reduced for both scenarios. In study 1, the HESS consisting of HE LIBs achieves approx. the same weight and volume as its ESS counterpart existing of high-power cells, but in the HESS the energy throughput Q_{TP} is reduced up to 55 %. In study 2 and 3, the HESS achieves approximately the same energy throughput Q_{TP} as its competitive battery-alone system, but weight and volume are reduced up to 30 %. In study 4, the energy throughput Q_{TP} is approximately 14 % higher in a HESS than in an ESS. Weight and volume are reduced up to 18 %. Considering P/E ratio, HESS shows higher P/E ratios than in its battery-alone counterpart in all studies, whereas the difference is decreasing from Gen1 to Gen3.

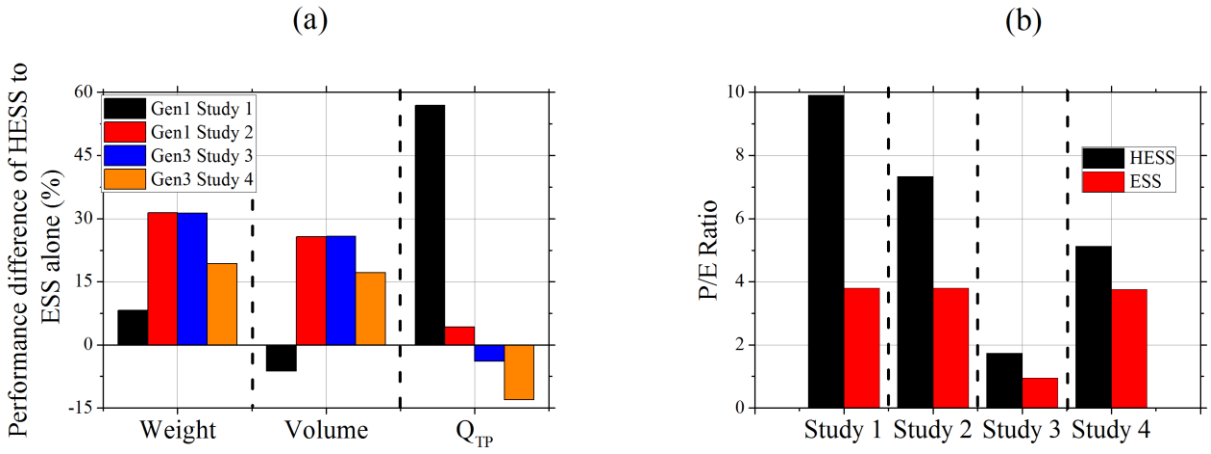

Figure 8: Comparison of passive HESS and ESS for Gen1 and Gen3 MHEV scenario; (a) Comparison of weight, volume, and energy throughput Q_{TP}; (b) P/E ratio of passive HESS and ESS within studies, resulting from maximum power and installed capacity of Table 5

6 Discussion

Experimental and model-based investigations have shown that passive HESS can be a suitable approach for nowadays and future generations of MHEV. However, several factors that influence the performance of a HESS have to be considered. The experimental campaign highlighted the influence of the HESS setup on its performance. Besides the influence of technology matching on cell level, improvements in power and energy density of the same composition up to a factor 5 on system level are possible. Furthermore, the characteristic of the pulse load profile influences the performance of a HESS. Shorter pulse lengths are leading to higher power densities. In general, a hybridization of LIB with LIC technologies leads to better performances than the other HESS. This is due to similar voltage levels and in the case of LFP and LIC_{PHC} due to similar voltage characteristics. In comparison to the LFP battery-alone system, an increase in power density up to a factor of 1.9 can be achieved. This comes with the drawback of a loss in energy density by 14 %.

The model-based campaign has proven that the used approach of a universal model for the different technologies is quite accurate on cell- and system level. It is clear that the model error is increasing from cell to system level as the number of external factors is increasing due to the increased complexity from ESS to a single cell. Still, the maximum error of 7 % within eight different HESS setups using six different technologies is quite satisfying when taken the high dynamics in current and voltage into account, that are existing within a passive HESS under pulse current load. In addition most model errors arise in low SOC area (<10 %) in which high voltage dynamics occur. The virtual concept study shows for both scenarios that the HESS approach is quite suitable for MHEV applications. The P/E ratio depends on the load profile, which is in line with the experimental results. Hence in study 4, the energy throughput Q_{TP} is approx. 14 % higher than in its competitive ESS. Impacts on aging will be analyzed in future studies along with standardized layout criteria for optimal HESS design.

7 Conclusion

In this work, passive HESS were investigated on cell and system level for different LIB and SC technologies within pulse load applications. The HESS performance was influenced by the technology match and also by the characteristics of the pulse profile. In addition, a universal model and its parameterization for LIB and SC technologies were presented and its validity on cell and system modeling was proven. A virtual concept study for two generations of MHEV was shown. In general, passive HESS show a better P/E ratio along with less necessary weight and volume than competitive battery-only ESS especially in high dynamic profiles. For pure electric driving scenarios, passive HESS still show a better P/E ratio but LIBs have to endure a higher energy throughput than its competitive battery-alone ESS. Impacts on aging behavior shall be part of further studies.

Acknowledgments

The authors thank Dr. Anna Smith and her research group from Institute for Applied Materials at Karlsruhe Institute of Technology for supplying cell data and also the necessary test environment and equipment. We also would like to thank Manuel Baena and Alexis Kalk from Institute of Electrical Engineering at Karlsruhe Institute of Technology for their support in developing and assembling the 48 V prototypes and its BMS.

References

[1] The Idaho National Laboratory, "U.S. Department of Energy Vehicle Technologies Program Battery Test Manual For 48 Volt Mild Hybrid Electric Vehicles," 2017. [Online]. Available: https://inldigitallibrary.inl.gov/sites/sti/sti/7364006.pdf.

[2] E. Degenhart, "Powertrain Review Powertrain Strategy 2020 +." [Online]. Available: https://www.continental-corporation.com/resource/blob/33902/50729be3c974864761524b7de1a8f625/2017-04-25-presentatione-powertrain-strategy-data.pdf [Accessed: 10-Oct-2018].

[3] Y. Chuan, C. Mi, and M. Zhang, "Comparative study of a passive hybrid energy storage system using lithium ion battery and ultracapacitor," *World Electr. Veh. J.*, vol. 5, no. 1, pp. 83–90, 2012.

[4] K. Naoi, S. Ishimoto, J. Miyamoto, and W. Naoi, "Second generation 'nanohybrid supercapacitor': Evolution of capacitive energy storage devices," *Energy Environ. Sci.*, vol. 5, no. 11, p. 9363, 2012.

[5] D. P. Dubal, O. Ayyad, V. Ruiz, and P. Gómez-Romero, "Hybrid energy storage: The merging of battery and supercapacitor chemistries," *Chem. Soc. Rev.*, vol. 44, no. 7, pp. 1777–1790, 2015.

[6] D. Cericola and R. Kötz, "Hybridization of rechargeable batteries and electrochemical capacitors: Principles and limits," *Electrochim. Acta*, vol. 72, pp. 1–17, 2012.

[7] D. Cericola, P. W. Ruch, R. Kötz, P. Novák, and a. Wokaun, "Simulation of a supercapacitor/Li-ion battery hybrid for pulsed applications," *J. Power Sources*, vol. 195, no. 9, pp. 2731–2736, 2010.

[8] A. Kuperman and I. Aharon, "Battery-ultracapacitor hybrids for pulsed current loads: A review," *Renew. Sustain. Energy Rev.*, vol. 15, no. 2, pp. 981–992, 2011.

[9] R. a. Dougal, S. Liu, and R. E. White, "Power and life extension of battery-ultracapacitor hybrids," *IEEE Trans. Components Packag. Technol.*, vol. 25, no. 1, pp. 120–131, 2002.

[10] C. E. Holland, J. W. Weidner, R. a. Dougal, and R. E. White, "Experimental characterization of hybrid power systems under pulse current loads," *J. Power Sources*, vol. 109, no. 1, pp. 32–37, 2002.

[11] D. Andre, S.-J. Kim, P. Lamp, S. F. Lux, F. Maglia, O. Paschos, and B. Stiaszny, "Future generations of cathode materials: an automotive industry perspective," *J. Mater. Chem. A*, vol. 3, no. 13, pp. 6709–6732, 2015.

[12] H. Budde-Meiwes, J. Drillkens, B. Lunz, J. Muennix, S. Rothgang, J. Kowal, and D. U. Sauer, "A review of current automotive battery technology and future prospects," *Proc. Inst. Mech. Eng. Part D J. Automob. Eng.*, vol. 227, no. 5, pp. 761–776, 2013.

[13] S. M. Mousavi G. and M. Nikdel, "Various battery models for various simulation studies and applications," *Renew. Sustain. Energy Rev.*, vol. 32, pp. 477–485, 2014.

[14] A. Seaman, T. S. Dao, and J. McPhee, "A survey of mathematics-based equivalent-circuit and electrochemical battery models for hybrid and electric vehicle simulation," *J. Power Sources*, vol. 256, pp. 410–423, 2014.

[15] L. Zhang, Z. Wang, X. Hu, F. Sun, and D. G. Dorrell, "A comparative study of equivalent circuit models of ultracapacitors for electric vehicles," *J. Power Sources*, vol. 274, pp. 899–906, 2015.

[16] H.-G. Schweiger, O. Obeidi, O. Komesker, A. Raschke, M. Schiemann, C. Zehner, M. Gehnen, M. Keller, and P. Birke, "Comparison of several methods for determining the internal resistance of lithium ion cells.," *Sensors (Basel).*, vol. 10, no. 6, pp. 5604–25, Jan. 2010.

[17] M. Dubarry, N. Vuillaume, and B. Y. Liaw, "From single cell model to battery pack simulation for Li-ion batteries," *J. Power Sources*, vol. 186, no. 2, pp. 500–507, 2009.

Authors

Thorsten Grün was born in Weert, Netherlands. He received the Dipl.-Ing degree in power systems technology from Clausthal University of Technology, Clausthal, Germany, in 2014. Since 2014 he is working at the Karlsruhe Institute of Technology, Karlsruhe, Germany. His research interests include the experimental and model-based investigation of lithium-ion batteries and supercapacitors on cell and system level and the design of hybrid storage systems.

Martin Doppelbauer was born in Altenhundem, Germany. He received the Dipl.-Ing. and Dr.-Ing. degrees in electrical engineering from the University of Dortmund, Dortmund, Germany, in 1990 and 1995, respectively.

He has worked with the companies Danfoss Bauer, Esslingen, and SEW Eurodrive, Bruchsal, Germany, as a Senior Manager for electric motor development. He has been holding the Professorship for hybrid electric vehicles at the Karlsruhe Institute of Technology, Karlsruhe, Germany, since 2011.